Shear Wave Splitting of the 2018 Lombok Earthquake Aftershock Area, Indonesia

Annisa Trisnia Sasmi (trisnia24@gmail.com)
Institut Teknologi Bandung https://orcid.org/0000-0003-4000-9379

Andri Dian Nugraha
Institut Teknologi Bandung

Muzli Muzli
Agency for Meteorology Climatology and Geophysics: Badan Meteorologi Klimatologi dan Geofisika

Sri Widiyantoro
Institut Teknologi Bandung

Syuhada Syuhada
LIPI Pusat Penelitian Fisika

Faiz Muttaqy
Institut Teknologi Bandung

Zulfakriza Zulfakriza
Institut Teknologi Bandung

Shengji Wei
NTU EOS: Nanyang Technological University Earth Observatory of Singapore

Awali Priyono
Institut Teknologi Bandung

Haunan Afif
Center for Volcanology and Geological Hazard Mitigation: Pusat Vulkanologi dan Mitigasi Bencana Geologi

Pepen Supendi
Agency for Meteorology Climatology and Geophysics: Badan Meteorologi Klimatologi dan Geofisika

Yayan Mi'rojul Husni
Institut Teknologi Bandung

Billy S Prabowo
Institut Teknologi Bandung

Achmad Fajar Narotama Sarjan
Institut Teknologi Bandung

Research Article

Keywords: 2018 Lombok earthquake, rupture, shear wave splitting, fast polarization direction, delay time

Posted Date: February 7th, 2022

DOI: https://doi.org/10.21203/rs.3.rs-1317712/v1

Shear Wave Splitting of the 2018 Lombok Earthquake Aftershock Area, Indonesia

Annisa Trisnia Sasmi[1], Andri Dian Nugraha[2], Muzli Muzli[3,4], Sri Widiyantoro[2,5], Syuhada Syuhada[6], Faiz Muttaqy[1], Zulfakriza Zulfakriza[2], Shengji Wei[3], Awali Priyono[2], Haunan Afif[7], Pepen Supendi[4], Yayan Mi'rojul Husni[8], Billy S Prabowo[8], Achmad Fajar Narotama Sarjan[1]

[1]Geophysical Engineering, Faculty of Mining and Petroleum Engineering, Institut Teknologi Bandung, Bandung, Indonesia

Email: *trisnia24@gmail.com*

[2]Global Geophysics Research Group, Faculty of Mining and Petroleum Engineering, Institut Teknologi Bandung, Bandung, Indonesia

[3]Earth Observatory of Singapore/Asian School of the Environment, Nanyang Technological University, Singapore

[4]Meteorology, Climatology, and Geophysics Agency (BMKG), Jakarta, Indonesia

[5]Faculty of Engineering, Maranatha Christian University, Bandung 40164, Indonesia

[6]Research Center for Physics, National Research and Innovation Agency (BRIN), South Tangerang, Indonesia

[7]Center for Volcanology and Geological Hazard Mitigation (PVMBG), Bandung, Indonesia

[8]Laboratory of Volcanology and Geothermal, Faculty of Mining and Petroleum Engineering, Institut Teknologi Bandung, Bandung, Indonesia

Abstract Lombok is one of the islands in the transitional zone from the Sunda Arc to the Banda Arc, Indonesia. In the mid-2018, the island of Lombok was shaken by a series of strong earthquakes, started with a magnitude 6.4 earthquake on July 29, 2018 followed by

earthquakes on August 5 (M 7.0), August 9 (M 5.9), and August 19 (M 6.3 and 6.9). Some researchers suggested that this phenomenon occurred due to a segmentation rupture in the northern part of Lombok Island.

This study aims to obtain information on the distribution of the Lombok earthquake rupture zone 2018, through Shear Wave Splitting (SWS) study. Splitting, or S-wave separation, occurs when the S-wave passes through an anisotropic medium. The S wave is split into fast and slow S waves with almost orthogonal polarizations and has parameters such as delay time and polarization direction of the fast S wave. To determine the SWS parameters, we used a Lombok earthquake aftershock data set recorded from 4 August to 9 September 2018, using 16 seismographic stations. The steps taken to obtain the SWS parameters are event selection, windowing using short time Fourier transform, and rotation-correlation process. The results of the SWS analysis indicate that the fast polarization directions probably have a linkage with the local fault system and the fault related to the Lombok earthquake rupture zone.

Keywords: 2018 Lombok earthquake, rupture, shear wave splitting, fast polarization direction, delay time

1. Introduction

In an anisotropic medium, shear waves tend to be polarized into approximately orthogonal fast (S_{fast}) and slow (S_{slow}) directions (Crampin et al., 1978). The phenomenon of shear wave splitting (SWS) can be characterized by measuring the time delay between the two polarized shear waves (δt) and S_{fast} polarization direction (ϕ). There are three anisotropy mechanisms that can generate SWS phenomenon: stress induced anisotropy, intrinsic anisotropy, and structure anisotropy. Stress-induced anisotropy can be described as the preferential

orientation of the open microcracks filled with fluid, under the influence of an active stress field (Boness and Zoback, 2006). Thus, the pattern of compressional strain direction in a region may affect the preferred direction of local microcracks. Consequently, stress-induced anisotropy controls the S_{fast} to propagate in a similar direction to the compressional strain of the area. For the second case, intrinsic anisotropy is defined as anisotropy due to the alignment of anisotropic minerals within the rock mass (Mainprice and Nicolas, 1989; Boness and Zoback, 2006). For the last mechanism, structure induced anisotropy is seismic anisotropy related to macroscopic crack alignment such as fault or strike slip (Zhang et al., 2007; Tadokoro and Ando, 1999), and sedimentary bedding system (Valcke et al., 2006; Kern and Wenk, 1990). In this case, structure induced anisotropy causes S_{fast} polarized parallel to the main strike of the anisotropic medium.

SWS analysis has been applied for seismic anisotropy studies either in the crust or mantle (e.g., Audet, 2014; Boness and Zoback, 2006). In the crustal regime, SWS is usually generated by the presence of local faults or sedimentary layering systems, and observable from near field seismic stations (e.g. Crampin and Peacock, 2008; Chang et al., 2009). Meanwhile, alignment of anisotropic minerals deformed through dislocation creep may produce SWS phenomenon in the mantle region. In this research, SWS analysis was applied for studying crustal anisotropy in Lombok Island region, Indonesia, using local earthquake waveforms extracted from the local temporary seismic stations.

Lombok Island is located near the border area between the Sunda Arc and the Banda Arc tectonic systems, Indonesia. The seismicity around Lombok Island is mainly governed by two tectonic arrangements around the area: the subduction zone in the south (Hamilton, 1977; 1979), and the back arc thrust system in the north (Hamilton, 1977, 1979; Silver et al., 1983). In addition, Lombok Island is flanked by the Lombok Strait Strike Slip Fault in the west, and

the Sumbawa Strait Shear Fault (Sumbawa Strait Strike Slip Fault) in the east (Irsyam et al., 2017). On July 29 2018, an earthquake of M 6.4 hit Lombok Island (BMKG, 2019). Another series of significant earthquakes also occurred on August 5 (M 7.0), August 9 (M 5.9) and August 19 (M 6.3 and M 6.9). Indonesian Agency of Meteorology, Climatology, and Geophysics or BMKG (2019) reported that the hypocenters of these significant earthquakes were mostly concentrated in the north of Lombok Island. The significant earthquakes that occurred several times were indicated as the result of segmentation ruptures formed before the occurrence of a strong earthquake (Wang et al., 2020; Sasmi et al., 2020). Salman et al. (2020) using InSAR data also explained that the significant earthquake sequences came from different hypocenters, and formed a rupture of a thrust fault that tilted to the south. This earthquake sequence might trigger secondary disasters such as landslides (Ferrario, 2019). In addition, it is suggested that the 2018 Lombok earthquake might cause a volumetric expansion in the shallow magma plumbing system at Rinjani volcano, which might affect the volcanic activity in the future (Salman et al., 2020).

Information related to the regional stress field around the Lombok Island is less studied, but the strain rate analysis from Bock et al. (2003) shows that the regional strain rate in the Sunda – Banda Arc transition zone is mostly oriented around NE-SW, roughly 35-40°. On the other hand, the 2018 Lombok earthquake caused fault segmentation with a different strike orientation. The focal mechanism analysis of the regional seismic network (Salman et al., 2020) indicates an east-west relative strike orientation between 85.4880° - 91.5725° of the Lombok earthquake fault system. For this reason, we implemented a crustal anisotropy study to prove whether crustal seismic anisotropy in the Lombok region is more influenced by the regional strain rate or the local fault system associated with the 2018 Lombok earthquake rupture zone. To examine this issue, we utilized 2018 Lombok aftershock data recorded by temporary seismic stations around this region. The aim of the study is to distinguish between

stress and structure-controlled anisotropy at distinct locations located within the 2018 Lombok earthquake area. Thus, this analysis may help to provide better knowledge about crustal anisotropy mechanisms around the region and to substantiate the deformation process related to the 2018 Lombok earthquake.

2. Seismic Network and Dataset

The SWS analysis was carried out using waveforms from local events recorded by 16 temporary seismic stations (Fig. 1) around Lombok Island from 4 August to 9 September 2018 (Sasmi et al., 2020). There were several stages of routine data processing that must be prepared before conducting SWS analysis, including selecting waveform data, equalizing sampling frequency, and instrument correction. In the first stage, we selected the data based on these criteria: 1) The data must be recorded by at least three seismic stations, 2) The data has three component seismograms (Vertical, E-W, N-S), 3) The waveform data must have clear S wave arrival. This selection process yielded a total of 3259 aftershocks that met the selection criteria for the SWS analysis. The number of S phases from these events was 17807. Most of the events were distributed around LM-09 station which is located near the source of the main earthquake on 19 August. The hypocenter depth of the recorded events varied from 0 to 68 km, and most of them were concentrated at the depth of 25-30 km (Fig. 5b). The hypocenter locations were initially determined using non-linear method, and then relocated using double-difference method (Sasmi et al., 2020).

To avoid the distortion effect of S wave phase at the free surface (Liu et al., 1997), we eliminated the shear waves with incidence angles greater than 40°, a typical cut-off value in SWS analysis (e.g. Araragi et al., 2015; Kanaujia et al., 2019). Nuttli (1961) explained that for a homogeneous half-space with 0.25 Poisson's ratio value, the critical angle is 35° from

vertical. In this research, we tolerated this angle to 40°to prevent the rejection of too much useful data. We then applied a 0.2-4 Hz bandpass filter to remove the effect of seismic noise.

3. Method

To determine the SWS parameters, we initially chose the appropriate waveform window length. The windowing process in the SWS analysis is applied using the Short Time Fourier Transform (STFT) analysis (Nawab and Quaiteri, 1998), for the sample area of 0.4 s around the arrival time of the wave phase. The aim of this process is to determine the dominant frequency from each waveform sampling zone. From the dominant frequency, the signal period will be obtained which then becomes a reference in the cross-correlation process. The windowing waveform process is one of the important steps in SWS analysis, because the duration length of the waveform affects the cross-correlation results between S_{fast} and S_{slow} wave phases.

As shown in Fig. 2, parameters δt and ϕ were then obtained from the results of cross-correlation or Rotation-Correlation (RC), to the S_{fast} and S_{slow} phases which have been rotated into the radial and tangential directions (Bowman and Ando, 1987; Vecsey et al., 2008). The cross-correlation process is carried out by varying the values of δt and ϕ in each of the S wave phase pairs. The increment value of δt used on the cross-correlation was adjusted to the data sampling interval, which is 100 ms. This process also searched all possible values of ϕ parameter from 0° to 180° with an interval of 1°. From the cross-correlation results, the correlation coefficient value will be obtained and form a Cross Correlation Coefficient (CCC) contour pattern. The selected splitting parameters for each event were obtained from the contour coordinates with the highest CCC value, with δt on the y-axis and ϕ on the x-axis.

4. Delay Time and Fast Polarization Analysis

There are several factors that affect the variation of the SWS polarization direction value, such as the dimensions and orientation of the subsurface anisotropic material, the presence of anisotropic mineral layers, the intensity of fractures in the medium, the presence of rock layers, etc (e.g. Crampin et al., 1986, Shelley et al., 2014). In the earth's crust, the direction of ϕ and δt is generally very dependent on the presence of fractures, sedimentary layers, and the direction of the maximum horizontal stress. In tectonic active areas, the direction of S_{fast} tends to be parallel to the horizontal direction of the maximum stress (Crampin and Chastin, 2003). In addition, paleostress conditions can also contribute to the direction of ϕ (Blenkinsop, 1990). Kleinrock and Humphris (1996) stated that this condition occurs because the stress field tends to cause joint alignments, rock pores, and microcracks which can increase the degree of seismic anisotropy. The value of the δt is strongly controlled by the degree of anisotropy of the medium and also the intensity of the fracture. The δt will be smaller if the fracture density in the medium is low.

The average ϕ and δt values obtained from this study are summarized in Table 1. The SWS directional statistical analysis was performed following Mardia (1972) and Davis (1986). Based on the results of the rose diagram (Fig. 3) and Table 1, we observe that the fast polarizations at most of the observation stations tend to vary in some different areas. Eken et al. (2011) and Zhang et al. (2018) suggested that in the earth's crust, the ϕ at an observation station is relatively parallel to the strike of the local fault. Furthermore, the SWS studies conducted around the strike-slip fault area generally show that the ϕ at stations adjacent to the fault zone tends to be parallel to the strike of the fault (Audet, 2014; Boness and Zoback, 2006). This can be seen at several stations adjacent to the fault, such as the Sumbawa Strike Slip Fault (LM 09, LM 10, LM 11) and the Lombok Strike Slip Fault (LM 14, LM 15, LM 16, LM 01), with a range of value ~40°, equal to the strikes of the Lombok Strike Slip Fault and Sumbawa Strike Slip Fault. Syuhada et al. (2017) conducted SWS analysis in the

Lombok and Sumbawa area using a regional seismograph network, and obtained a similar direction for stations located in the West Lombok and West Sumbawa. Resemblant conditions are also seen at several stations adjacent to the aftershock hypocenter, such as LM 03, LM 04, LM 05, LM 06. At these four stations, the ϕ is relatively oriented in the E-W direction, with values ranging from 85.48° to 93.03°. Salman et al. (2020) estimated the fault orientation of the Lombok earthquake rupture area using the waveform inversion of the regional seismic network, and obtained the strike direction range similar to the ϕ of our result. Thus, it can be concluded that the SWS parameters at several stations distributed in North Lombok are related to the presence of the 2018 Lombok earthquake faults system.

Table 1. Result of SWS parameter measurement.

STATION NAME	AVERAGE OF Φ (DEGREE)	AVERAGE OF ΔT (*S*)
LM01	20.00 ± 17.93	0.24 ± 0.01
LM02	-46.13 ± 10.88	0.35 ± 0.09
LM03	88.01 ± 42.00	0.27 ± 0.07
LM04	93.03 ± 14.96	0.19 ± 0.08
LM05	91.57 ± 37.90	0.19 ± 0.07
LM06	85.48 ± 27.62	0.24 ± 0.08
LM07	33.14 ± 20.83	0.23 ± 0.03
LM08	-23.43 ± 25.41	0.26 ± 0.09
LM09	40.30 ± 35.09	0.32 ± 0.02
LM10	38.71 ± 42.89	0.33 ± 0.05
LM11	30.55 ± 10.17	0.24 ± 0. 08
LM12	27.43 ± 22.30	0.28 ± 0.09
LM13	25.73 ± 21.46	0.21 ± 0.05
LM14	-10.86 ± 10.89	0.34 ± 0.07
LM15	9.81 ± 5.08	0.23 ± 0.03

LM16	35.98 ± 19.28	0.26 ± 0.01

Other than the local fault structure, local-tectonic stress conditions may also affect the direction of ϕ resulting from this study. In this case, Syuhada et al. (2017) conducted SWS analysis in the Sunda-Banda Arc transition zone and obtained the ϕ direction pattern with NE-SW orientation in the areas of Lombok, Sumbawa, and East Nusa Tenggara islands. Crampin (1978) proposed that seismic anisotropy in the crust is generally caused by microcracks associated with the local-tectonic stress. Stress induced anisotropy causes the fast orientation to be aligned parallel to the compressional strain. This previous anisotropy result is consistent with the strain rate analysis (Bock et al. 2003) showing that the direction of the regional strain rate axis in the Lombok area is generally oriented in NE-SW direction. The influence of this local structure in this region will be discussed in the following section.

5. The Influence of Structure Induced Anisotropy

To substantiate and analyse the spatial variations of fast polarization direction, we adapted the shear wave splitting spatial averages algorithm developed by Johnson et al. (2011); Johnson and Savage (2012). In this case, the ϕ values were determined to every spatial grid block passed by a certain number of rays, and weighted inversely to the square of the distance from the station. The minimum block size assigned was 10 km containing 10-80 rays in each grid block. If the standard deviation was greater than 30° or the raypath density was too low (<10), the result of ϕ spatial average would not be plotted in the block. The mean fast direction ϕ was then calculated using circular statistics.

We analysed the complexity of the spatially averaged ϕ as shown by Fig. 4. Bock et al. (2003) reported that the compressional strain rate axes are generally oriented around 35° – 40° in Sunda-Banda Arc Transitional Zone. Conversely, our results show spatial variations in

fast directions reflecting variations in anisotropic sources around this area. Furthermore, the polarization direction > 40° observed in our finding are probably caused by perturbation either due to the presence of local fault and local stress field, or the preferred orientation of anisotropic minerals (e.g. Hiramatsu and Iidaka, 2015).

In Lombok Strike Slip Fault and Sumbawa Strike Slip Fault, the ϕ values are generally parallel to the strike of the two faults, which is around N 30°E (Irsyam et al., 2017). Around Sumbawa Island particularly in the oceanic region, the spatial means of fast directions are also in the NE-SW direction. This condition suggests that crustal anisotropy around this area may be controlled by the opening of microcracks related to the local tectonic stress (Syuhada et al., 2017; Bock et al., 2003). Meanwhile towards the northern region of Lombok Island, the spatially averaged fast polarizations are predominantly around W–E. This condition most likely occurs due to the lineament of the Flores Back Arc Thrust, or the fault segmentation system caused by the 2018 Lombok earthquake, which shows a similar lineament (Salman et al., 2020). This resemblant pattern can be observed in the seismograph stations located to the north of Lombok Island (LM 03, LM 04, LM 05, LM 06). In the central area of Lombok Island which is adjacent to Mount Rinjani, the pattern of ϕ values is disrupted in various directions. This is probably due to the presence of volcanic activity in Mount Rinjani contributing to the anisotropy sources around this area. In the volcanic area, the stress around the crust area tends to suppress the magma reservoir from various directions, causing cracks in random strikes, and the cracks are filled with fluid. This condition can affect the distribution of SWS parameters in the volcanic areas, especially for the direction of ϕ which tends to be more scattered or complex. This condition is also illustrated in seismic station LM07 where the rosette diagram of ϕ shows a scattered distribution.

In Fig. 5b, we can see that the earthquake hypocenters are mainly distributed to the depth of 15-30 km. Fig. 5a shows δt variation for every depth increment. This Fig depicts that the higher δt is mainly distributed at the first 15 km depth. This pattern also shows that δt is independent with the increasing of focal depth. This condition suggests that the possible dominant source of anisotropy is located in the upper crust zone, approximately 15-20 km. Syuhada et al. (2017) also found through SWS analysis using the regional seismic station in the Sunda-Banda arc transition zone that the anisotropy in that region is confined down to 15-25 km depth. Our finding is also comparable with the result of Kaneshima (1990) who reported higher δt observed for events with focal depth up to 15 km, suggesting that crustal anisotropy existed in the upper 15 to 25 km depth of the crust in Japan.

This may be related to the influence of the crack zone formed during the 2018 Lombok significant earthquake (Sasmi et al., 2020; Afif et al., 2021; Priyono et al., 2021; Wang et al., 2020; Salman et al., 2020). Sasmi et al. (2020) explained that the 2018 Lombok earthquake aftershocks were mostly distributed to the depth of < 20 km with an average hypocenter slope of ~30^{o} and thought to be related with the rupture zone of 2018 Lombok earthquake. These significant events of earthquake were suspected as a result of the oceanic crust slabbed to the north of Lombok Islands and caused fault segmentation (Sasmi et al., 2020; Afif et al., 2021; Priyono et al., 2021; Wang et al., 2020; Salman et al., 2020; Yang et al., 2020; Lythgoe et al., 2021). The results from these studies confirm that the lack of correlation between event depths and δt suggests the shallow anisotropic fabrics may control the main possible sources of anisotropy in this area. We suggest that inclusion, either from fluid-filled cracks from Mt. Rinjani volcanic system (Afif et al., 2021; Sundhoro et al., 2000), or fluid related to the subduction system of oceanic crust in the north of Lombok (Afif et al., 2021; Priyono et al., 2021; Yang et al., 2020) contributes to the crustal anisotropy beneath the Lombok Island. The

presence of fluid in the microcrack systems can preclude the microcracks to close producing higher degree of anisotropy.

6. Temporal Variation Analysis

Analysis of temporal variation in splitting parameters is a recommended method for predicting the occurrence of earthquakes (e.g., Crampin et al., 2008; Aster and Shearer, 1991; Syuhada et al., 2017) and volcanic eruptions (e.g., Miller and Savage, 2001; Gerst and Savage, 2004; Gerst, 2003). The microcrack geometry changing prior to an earthquake or volcanic eruption can affect the change in splitting parameters. Crampin and Peacock (2008) reported that the temporal variations in δt have been observed after the occurrence of large earthquakes showing the systematic pattern between the event magnitudes and delay time. Saiga et al. (2003) also reported that there is a relation between the changes in SWS parameters and the expanding crack density due to the coseismic stress changes after the Aichi-Ken Tobu earthquake. Furthermore, temporal variations of ϕ have been utilized as a possible tool to analyse the stress change beneath Mt. Ruapehu, New Zealand, prior to the volcanic eruption (Gerst and Savage, 2004). They suggested that the changes in splitting parameters around this region are associated with the pressure changes originating from the magma chamber. Temporal variations in SWS parameters can also be employed to detect the fluid-saturated microcracks zone (Crampin and Peacock, 2008), and the alteration of microcrack geometry related to the intermediate earthquakes (Crampin et al., 2008).

We display two examples of stations that probably exhibit temporal variations in SWS parameters at LM05 and LM06 stations. Fig. 6 shows the temporal variation in time delay at station LM05 and LM06. We applied 10-window-moving averages of splitting delay time. We observe interesting patterns of the delay-time-moving mean that are probably correlated to the magnitude variation of the events. The two stations indicate correlation between

temporal variations in δt and the earthquake magnitudes. In general, the pattern of δt seems to increase slightly following the significant earthquake on August 9th. The increasing trend is also clearly seen after the August 19 earthquake, given that on August 19, 2018 there were two fairly large earthquakes (M 6.3 and M 6.9). The increasing pattern in delay time is probably caused by the crack aspect ratio pertained to the stress change subsequent to a significant earthquake (Crampin and Peacock, 2008). This probably happened because of the large deformation formed after the August 19 earthquake. Wang et al. (2020) explained that there is a stress increase surround the east of the 19 August seismogenic fault, seen by the result of coulomb stress analysis. The stress was thought to be accumulated before the August 19 earthquake and then released and resulted in slip movement generated M 6.3 and M 6.9 earthquake (Wang et al., 2020; Salman et al., 2020). On the other hand, the condition of the data is not yet sufficient to properly describe the temporal variation around August 7th. This was due to the incomplete seismographic network installed at the location on that date. Although we are able to examine the variation of δt correlated with the event magnitudes, the temporal trend of ϕ is not obviously seen in any stations. The similar findings are also reported by Syuhada et al. (2017) which analysed the temporal variation of SWS parameters in adjacent areas using regional seismographic network data.

7. Conclusion

SWS parameter analysis and spatial averaging of fast azimuths have been carried out around the hypocenter area of the 2018 Lombok earthquake aftershock using 16 local seismographic network data. The results of the SWS measurements show that the ϕ distribution implies a consistency with the presence of local fault structures, such as the Lombok Shear Fault, Sumbawa Shear Fault, and the fault area due to the Lombok earthquake 2018. We also observed a relatively E-W trend of ϕ direction in the north of Lombok Island which is

consistent with the strike direction of fault formed after the 2018 Lombok Earthquake, and Flores Back Arc Thrust. The NNE fast azimuths observed in the west and east part of study area may also be associated with the presence of Lombok Strait Strike Slip Fault and Sumbawa Strait Strike Slip Fault. We suggest that the anisotropy sources beneath the 2018 Lombok Earthquake rupture zone are mainly controlled by the presence of fluid inclusion, which is suspected either from Mt. Rinjani magmatic activity or crack-filled fluid of Flores Oceanic Crust subduction system near the main source of the 2018 Lombok Earthquake. The δt versus depth graphic shows that the anisotropy structure is likely found in 15-20 km depth and consistent to Lombok earthquake source depth. The temporal variation in δt observed in this study may be correlated with the stress changes following the increasing trend of event magnitudes. Therefore, the anisotropy mechanism in this area is strongly presumed to be related to the structure-controlled anisotropy.

Authors's Contributions

ATS, ADN, MM, SW, SS, FM, ZZ, AP, HA, PS conceived the study; ATS, ADN, SW, SS, FM contributed to the writing of the manuscript; YMH, BSP, AFNS carried out the data acquisition process. All authors contributed to the preparation of the manuscript. All authors have read and approved the final manuscript.

Acknowledgements

We would like to thank our colleagues at Institut Teknologi Bandung (ITB), the Earth Observatory Singapore (EOS), and the Agency for Meteorology, Climatology, and Geophysics of Indonesia (BMKG) for their collaboration. We really appreciate D. Kusumawati, P.P. Rahsetyo, A. Ardianto, K.H. Palgunadi, and A. Luthfian for the fruitful discussions. Maps in this study were made by using the Generic Mapping Tools developed by Wessel and Smith (1995).

Competing Interests

We declare that we have no significant competing financial, professional or personal interests that might have influenced the performance or presentation of the work described in this manuscript.

Supplemental materials

The additional file regarding the explanation of the waveform windowing process using the Short Time Fourier Transform, as well as the spatial averaging method, are available.

Funding

We also express our gratitude for the PMDSU Batch IV scholarship program (2018) established by the Indonesian Ministry of Research, Technology, and Higher Education and for the support and research funding given to ATS; DIKTI (PDUPT) and World Class Research Funding (2021-2022) awarded to ADN.

References

Afif H, Nugraha AD, Muzli M, Widiyantoro S, Sahara DP, Riyanto A, Greenfield T, Puspito NT, Priyono A, Sasmi AT, Supendi P, Ardianto A, Syahbana DK, Rosalia S, Cipta A, Husni YM (2021) Local Earthquake Tomography of The Source Region of The 2018 Lombok Earthquake Sequence, Indonesia. Geophysical Journal International 226:1814–1823. https://doi.org/10.1093/gji/ggab189

Araragi KR, Savage MK, Ohminato T, Aoki Y (2015) Seismic anisotropy of the upper crust around Mount Fuji, Japan. Journal of Geophysical International

Aster RC and Shearer P (1991) High-frequency borehole seismograms recorded in the San Jacinto fault zone, Southern California, Part 1: polarizations. Bulletin of Seismological Society of America 81:1057–1080

Audet P (2014) Layered crustal anisotropy around the San Andreas Fault near Parkfield, California. Journal of Geophysical Research 120:3527–3543. https://doi.org/10.1002/2014JB011821

Badan Meteorologi, Klimatologi, and Geofisika (BMKG) (2019) Katalog Gempa Bumi Signifikan and Merusak Tahun 1821-2018. Pusat Gempa and Tsunami BMKG. *https://www.bmkg.go.id/gempabumi/katalog-gempabumi-signifikan.bmkg.* Accessed at September 2021

Blenkinshop TG (1990) Correlation of Palaeotectonics Fracture and Microfracture Orientations in cores with seismic anisotropy at Cajon Pass Drill Hole, Southern California. Journal of Geophysical Research 95**:**11143-11150

Bock Y, Prawirodirdjo L, Genrich JF, Stevens CW, McCaffrey R, Subarya C, Puntodewo SSO, Calais E (2003) Crustal motion in Indonesia from global positioning system measurements. Journal of Geophysical Research 108:2367, http://dx.doi.org/10.1029/2001JB000324

Boness N and Zoback M (2006) Mapping stress and structurally controlled crustal shear velocity anisotropy in California. Geology 34:825–828

Bowman JR and Ando M (1987) Shear-wave splitting in the upper-mantle wedge above the Tonga subduction zone. Geophysical Journal Research of Astronomical Society 88: 25–41. doi:10.1111/j.1365-246X.1987.tb01367.x

Chang ETY, Liang W-T, Tsai YB (2009) Seismic shear wave splitting in upper crust characterized by Taiwan tectonic convergence. Geophysical Journal International 177:1256–1264, https://doi.org/10.1111/j.1365-246X.2009.04110.x

Crampin S (1978) Seismic-wave propagation through a cracked solid: polarization as a possible dilatancy diagnostic. Geophysical Journal of the Royal Astronomical Society 53:3. https://doi.org/10.1111/j.1365-246X.1978.tb03754.x

Crampin S, Bamford D, Mcgonigle R (1978) Estimating crack parameters by inversion of P wave velocity-anisotropy. Geophysical Journal of the Royal Astronomical Society 53:173–173

Crampin S, Booth DC, Krasnova MA, Chesnokov EM, Maximov AB, Tarasov NT (1986) Shear-wave polarizations in the Peter the First Range indicating crack-induced anisotropy in a thrust-fault regime. Geophysical Journal International 84:401–412, https://doi.org/10.1111/j.1365-246X.1986.tb04362.x

Crampin S and Chastin S (2003) A review of shear wave splitting in the crack-critical crust. Geophysical Journal International 155:221–240. https://doi.org/10.1046/j.1365-246X.2003.02037.x

Crampin S, Gao Y, Peacock S (2008) Stress-forecasting (not predicting) earthquakes: a paradigm shift? Geology 36:427–430. http://dx.doi.org/10.1130/G24643A.1

Crampin S and Peacock S (2008) A review of the current understanding of seismic shear-wave splitting in the earth's crust and common fallacies in interpretation. Wave Motion 45:675–722. http://dx.doi.org/10.1016/j.wavemoti.2008.01.003

Davis J (1986) Statistics and data analysis in Geology. John Wiley and Sons

Eken T, Bulut F, Bohnhoff M, Can B, Aktar M, Dresen G (2011) Crustal Anisotropy in the Eastern Sea of Marmara Region in Northwestern Turkey. AGU Fall Meeting Abstracts 103:2170-. 10.1785/0120120156

Ferrario MF (2019) Landslide trigerred by multiple earthquakes: Insight from the 2018 Lombok (Indonesia) events. National Hazards 98 (2):575-592

Gerst A (2003) Temporal Changes in Seismic Anisotropy as a New Eruption Forecasting Tool? Victoria University of Wellington, New Zealand (M.Sc. thesis)

Gerst A and Savage MK (2004) Seismic anisotropy beneath Ruapehu volcano: a possible eruption forecasting tool. Science 306:1543–1547. http://dx.doi.org/10.1126/science.1103445

Hamilton, WB (1977) Subduction in the Indonesian region, in Island Arcs, Deep Sea Trenches and Back-Arc Basins. American Geophysical Union 15–31 Maurice Ewing Series 1

Hamilton, WB (1979) Tectonics of the Indonesian region. Technical Report 1078, United States Government Publishing Office

Hiramatsu Y and Iidaka T (2015) Stress state in the upper crust around the source region of the 1891 Nobi earthquake through shear wave polarization anisotropy. Earth, Planets and Space 67:52. DOI 10.1186/s40623-015-0220-4

Irsyam M, Widiyantoro S, Natawidjaya DH, Meilano I, Rudyanto A, Hidayati S, Triyoso W, Hanifa NR, Djarwadi D, Faizal L, Sunarjito S (2017) Peta sumber and bahaya gempa Indonesia tahun 2017. Pusat Penelitian and Pengembangan Perumahan and Permukiman, Kementerian Pekerjaan Umum and Perumahan Rakyat

Johnson JH, Savage MK, and Townend J (2011) Distinguishing between stress-induced and structural anisotropy at Mount Ruapehu volcao, New Zealand. Journal of Geophysical Research, Solid Earth. https://doi.org/10.1029/2011JB008308

Johnson JH and Savage MK (2012) Tracking volcanic and geothermal activity in the Tongariro Volcanic Centre, New Zealand, with shear wave splitting tomography. Journal of Volcanology and Geothermal Research 223-224 (2012): 1–10. doi:10.1016/j.jvolgeores.2012.01.017

Kanaujia J, Mitra S, Gupta SC, Sharma ML (2019) Crustal anisotropy from shear-wave splitting of local earthquakes in the Garhwal Lesser Himalaya. Geophysical Journal International 219:2013–2033. doi: 10.1093/gji/ggz404

Kaneshima S (1990) Origin of crustal anisotropy: shear wave splitting studies in Japan. Journal of Geophysical Research 97:11121–11133

Kern H and Wenk HR (1990) Fabric related velocity anisotropy and shear wave splitting in rocks from the Santa Rosa mylonite Zone, California. Journal of Geophysical Research 95

Kleinrock MC and Humphris SE (1996) Structural control on sea-floor hydrothermal activity at the TAG active mound. Nature 382:149–153

Liu Y, Crampin S, and Main I, (1997) Shear-wave anisotropy: spatial and temporal variations in time delays at Parkfield, Central California. Geophysics Journal International 130:771–785

Lythgoe K, Muzli M, Bradley K, Wang T, Nugraha AD, Zulfakriza Z, Widiyantoro S, Wei S (2021) Thermal squeezing of the seismogenic zone controlled rupture of the volcano-rooted Flores Thrust. Science Advances. doi: 10.1126/sciadv.abe2348

Mardia KV (1972) Statistics of Directional Data. Academic Press. https://doi.org/10.1016/C2013-0-07425-7

Mainprice D and Nicolas A (1989) Development of shape and lattice preferred orientations. Journal of Structural Geology. DOI:10.1016/0191-8141(89)90042-4

Miller V and Savage MK (2001) Changes in seismic anisotropy after volcanic eruptions: evidence from Mount Ruapehu. Science 293:2231–2233, http://dx.doi.org/10.1126/science.1063463

Nawab SH and Quaiteri TF (1988) Short Time Fourier Transform. Advanced Topics in Signal Processing, Prentice Hall, Englewood Cliffs, New Jersey

Nuttli O (1961) The effect of the Earth's surface on the S wave particle motion, Bulletin of Seismological Society of America 51:237–246

Priyono A, Nugraha AD, Muzli M, Ardianto A, Aulia AN, Prabowo BS, Zulfakriza Z, Rosalia S, Sasmi AT, Afif H, Sahara DP, Widiyantoro S, Wei S, Husni YM, Sarjan AFN, (2021) Seismic Attenuation Tomography From 2018 Lombok Earthquakes, Indonesia. Frontiers in Earth Science 9:639-692. doi: 10.3389/feart.2021.639692

Saiga A, Hiramatsu Y, Ooida T, Yamaoka K (2003) Spatial variation in the crustal anisotropy and its temporal variation associated with a moderate-sized earthquake in the Tokai region, central Japan. Geophysical Journal International 154:695–705, http://dx.doi.org/10.1046/j.1365-246X.2003.01998.x

Salman R, Lindsey EO, Lythgoe KH, Bradley K, Muzli M, Yun S-H, Chin ST, Tay CWJ, CostaF, Wei S, Emma H (2020) Cascading Partial Rupture of the Flores Thrust during the 2018 Lombok Earthquake Sequence, Indonesia. Seismological Research Letter XX:1–11. doi: 10.1785/ 0220190378

Sasmi AT, Nugraha AD, Muzli M, Widiyantoro S, Zulfakriza Z, Wei S, Sahara DP, Riyanto A, Puspito NT, Priyono A, Greenfield T, Afif H, Supendi P, Daryono D, Ardianto A, Syahbana DK, Husni YM, Prabowo BS, Sarjan AFN (2020) Hypocenter and Magnitude Analysis of Aftershocks of the 2018 Lombok Earthquakes, Indonesia, Using Local Seismographic Networks. Seismological Research Letter XX:1-11. doi: 10.1785/0220190348

Shelley A, Savage M, Williams C, Aoki Y, Gurevich B (2014) Modeling shear wave splitting due to stress-induced anisotropy, with an application to Mount Asama Volcano, Japan. Journal of Geophysical Research: Solid Earth 119:4269–4286. https://doi.org/10.1002/2013JB010817

Silver EA, Reed D, McCaffrey R, Joyodiwiryo Y (1983) Backarc thrusting in the Eastern Sunda Arc, Indonesia: a consequence of arc–continent collision. Journal of Geophysical Research 88:7429–7448

Sundhoro H, Nasution A, Simanjuntak J (2000) “Sembalun Bumbung geothermal area, Lombok Island, West Nusatenggara, Indonesia: an integrated exploration,” in Proceedings World Geothermal Congress 2000. Corpus ID: 195732099, Kyushu

Syuhada S, Hananto ND, Abdullah CI, Puspito NT, Anggono T, Yudistira T, Ramdhan M (2017) Crustal anisotropy along the Sunda-Banda arc transition zone from shear wave splitting measurements. Journal of Geodynamics 103:1–11

Tadokoro K and Ando M (1999) Evidence for rapid fault healing derived from temporal changes in S wave splitting. Geophysical Research Letter 29:1047, 10.1029/2001GL013644, 2002

Valcke SLA, Casey M, Lloyd GE, Kendall J-M, Fisher QJ (2006) Lattice preferred orientation and seismic anisotropy in sedimentary rocks, Geophysical Journal International 166:652–666

Vecsey L, Plomerova J, Babuska V (2008) Shear-wave splitting measurements — Problems and solutions. Tectonophysics 462:178–196

Wang C, Wang X, Xiu W, Zhang B, Zhang G, Liu P (2020) Characteristics of the Seismogenic Faults in the 2018 Lombok, Indonesia, Earthquake Sequence as Revealed by Inversion of InSAR Measurements. Seismological Research Letter XX:1–12. doi: 10.1785/0220190002

Wessel P and Smith WHF (1995) New version of the Generic Mapping Tools released. Eos, Transactions, American Geophysical Union 76:329

Yang X, Singh SC, Tripathi A (2020) Did The Flores Backarc thrust rupture offshore during the 2018 Lombok Earthquake sequence in Indonesia? Geophysical Journal International 221:758-768

Zhang H, Liu Y, Thurber C, Roecker S (2007) Three-dimensional shear-wave splitting tomography in the Parkfield, California, region. Geophysical Research Letter 34:L24308. doi:10.1029/2007GL031951

Zhang B, Zhang S, Wu T, Hua T (2018) Upper crustal anisotropy from local shear-wave splitting and crust-mantle coupling of Yunnan, SE margin of Tibetan Plateau. Geodesy and Geodynamics 9:302-311. ISSN 1674-9847, https://doi.org/10.1016/j.geog.2018.01.004

Figures:

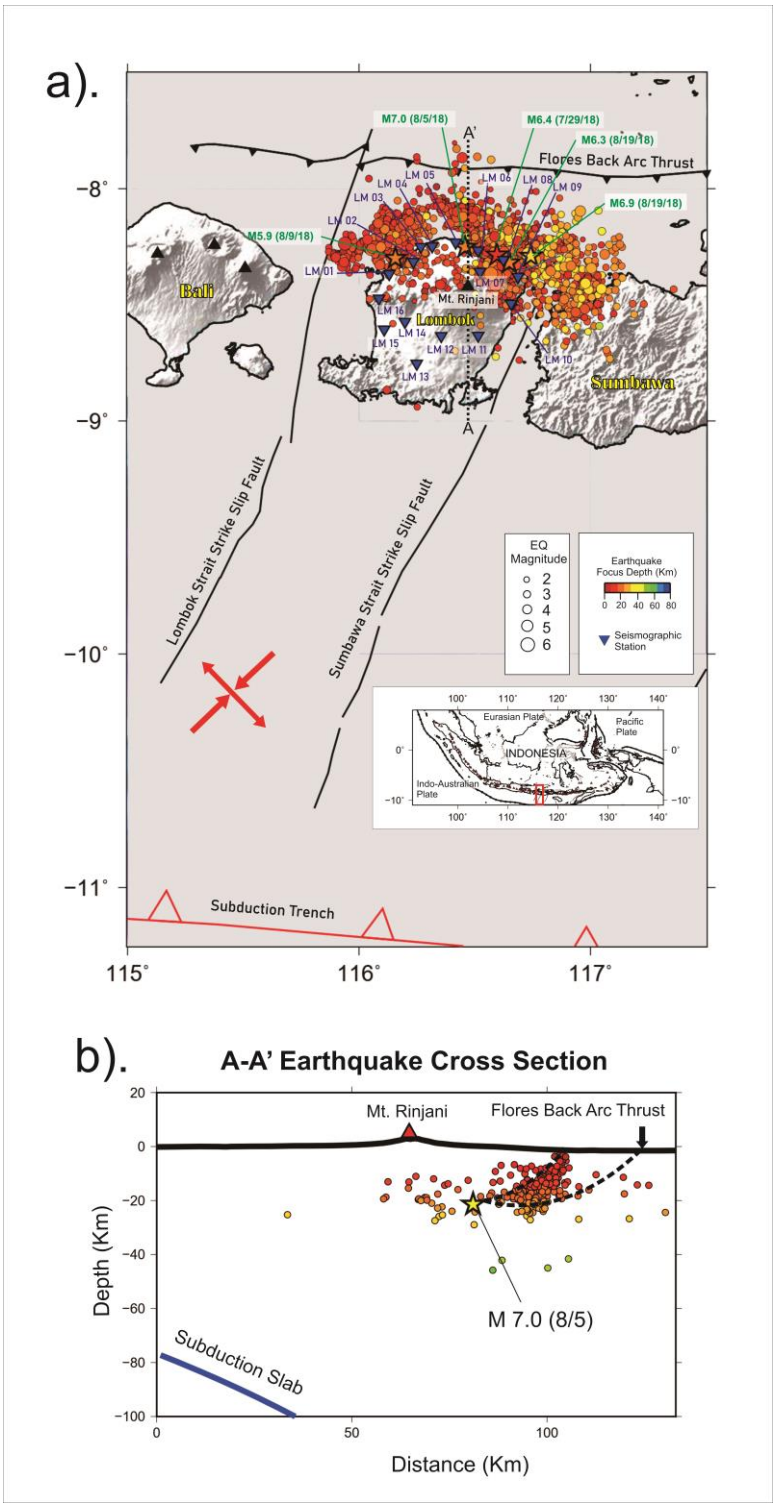
a).
M7.0 (8/5/18)
M6.4 (7/29/18)
M6.3 (8/19/18)
M6.9 (8/19/18)
M5.9 (8/9/18)
Flores Back Arc Thrust
LM 01
LM 02
LM 03
LM 04
LM 05
LM 06
LM 07
LM 08
LM 09
LM 10
LM 11
LM 12
LM 13
LM 14
LM 15
LM 16
Mt. Rinjani
Bali
Lombok
Sumbawa
A
A'
Lombok Strait Strike Slip Fault
Sumbawa Strait Strike Slip Fault
Subduction Trench
EQ Magnitude
2
3
4
5
6
Earthquake Focus Depth (Km)
0 20 40 60 80
Seismographic Station
Eurasian Plate
Pacific Plate
INDONESIA
Indo-Australian Plate
−8°
−9°
−10°
−11°
115°
116°
117°
b).
A-A' Earthquake Cross Section
Mt. Rinjani
Flores Back Arc Thrust
M 7.0 (8/5)
Subduction Slab
Depth (Km)
Distance (Km)
20
0
−20
−40
−60
−80
−100
0
50
100

Fig. 1. a) The location of the study area (red box on the inset map), overlaid with the 2018 Lombok earthquake aftershock hypocentre (circle), modified from Sasmi et al. (2020). The red arrows show compressional strain rate direction from Bock et al. (2003). The coloured symbol shows the hypocentres of significant earthquake. The dashed black line represents A-A' hypocentre cross section illustrated in 1b) (Sasmi et al., 2020). The black triangle shows the location of volcanoes. The map was plotted using Generic Mapping Tool (Wessel and Smith, 1995).

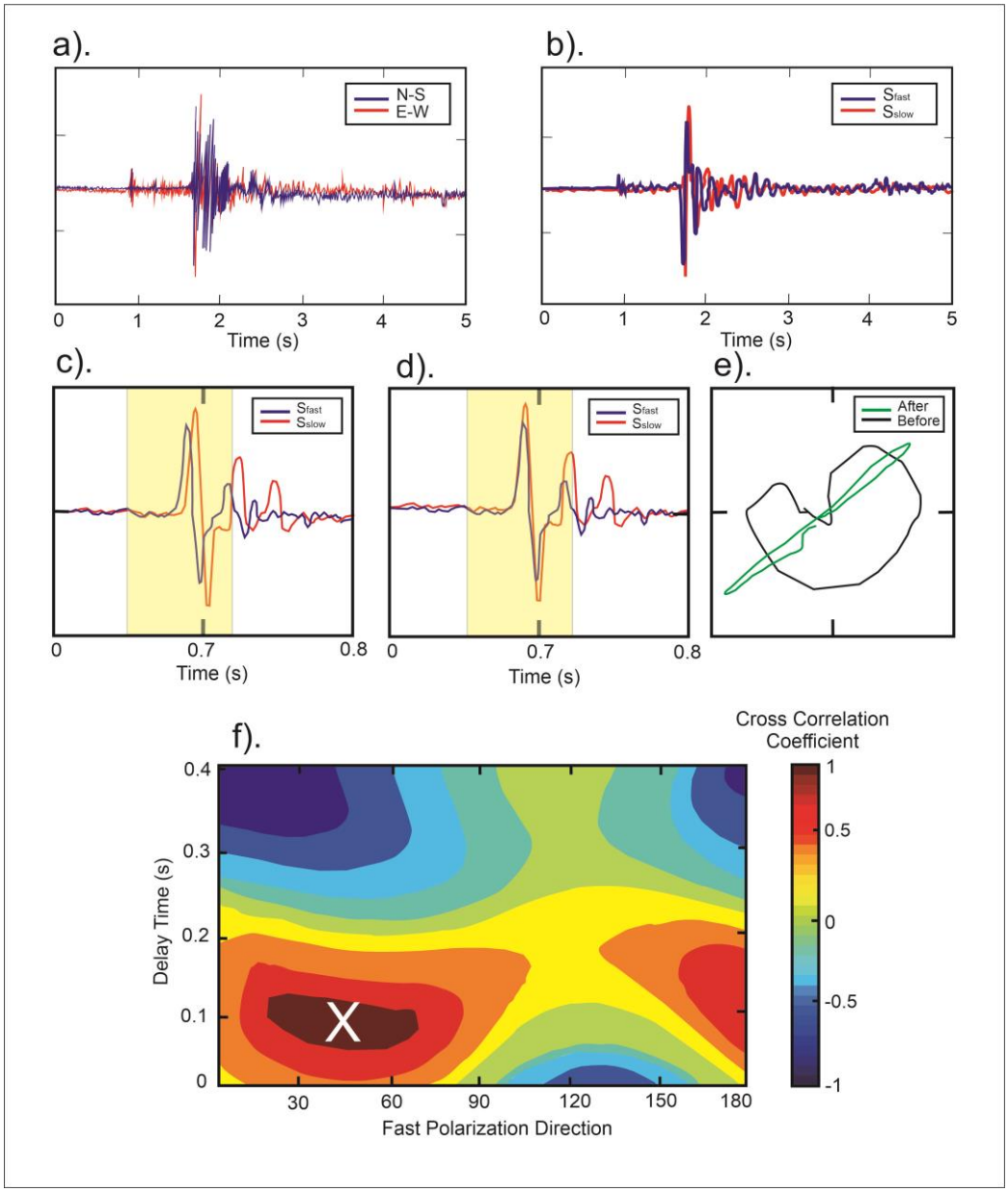

Fig. 2. a) An example of raw seismograph of N-S and E-W component of August 7 5:25 UTC event; b) Seismograph of 2a) that had been filtered using bandpass filter; c) Rotated seismograph shows similar shape of S_{fast} and S_{slow} waveform; d) Time-shifted seismograph; e) Hodogram of the seismograph particle motion, before and after the seismogram rotation process; f). An example of SWS parameter determination process using Rotated-correlation (RC) method for event in Fig. 2a).

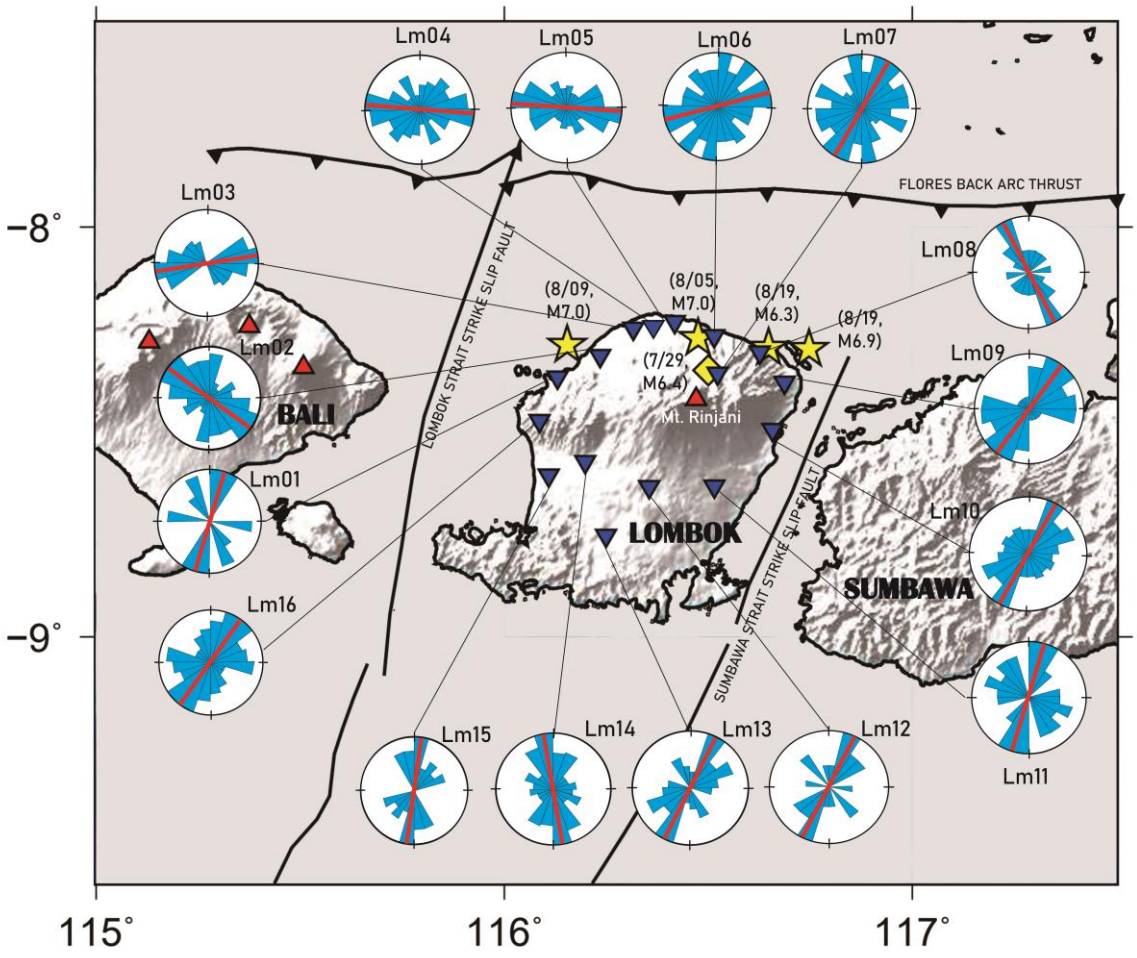

Fig. 3. Rosette diagram distribution of ϕ direction parameter in each seismograph station, shown by circles with blue bars. The red lines show the average value of ϕ. The yellow stars represent the epicentre of significant earthquakes (Sasmi et al., 2020), and the yellow diamond show the epicentre of M 6.4 July 29, 2018 earthquake (BMKG, 2019). The blue inverted triangles indicate the distribution of seismograph station.

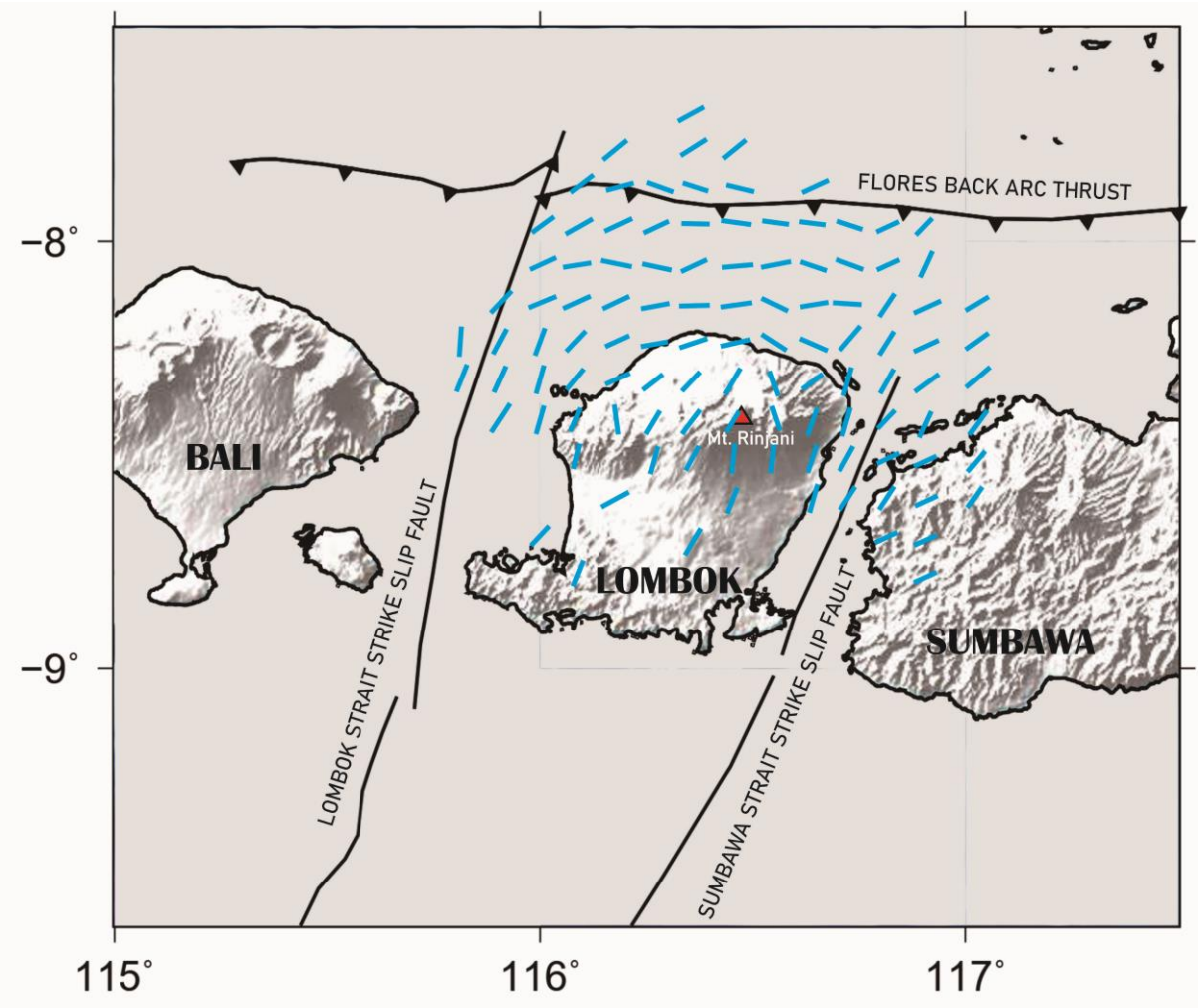

Fig. 4. The distribution of spatially averaged ϕ in 10 x 10 km grid size (blue lines).

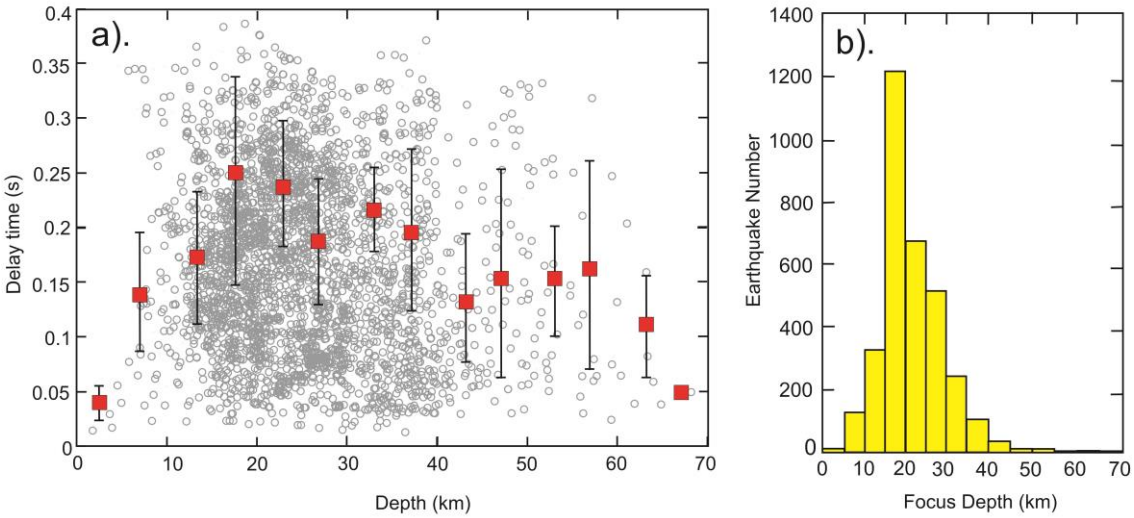

Fig. 5. a) Distribution of delay time respect to earthquake focus depth, shown by grey circles. The red rectangles signify the average of delay time in every 5 km depth increment. The underlying black lines denote the standard deviation of each red rectangle; b) Histogram of earthquake number versus earthquake focus depth.

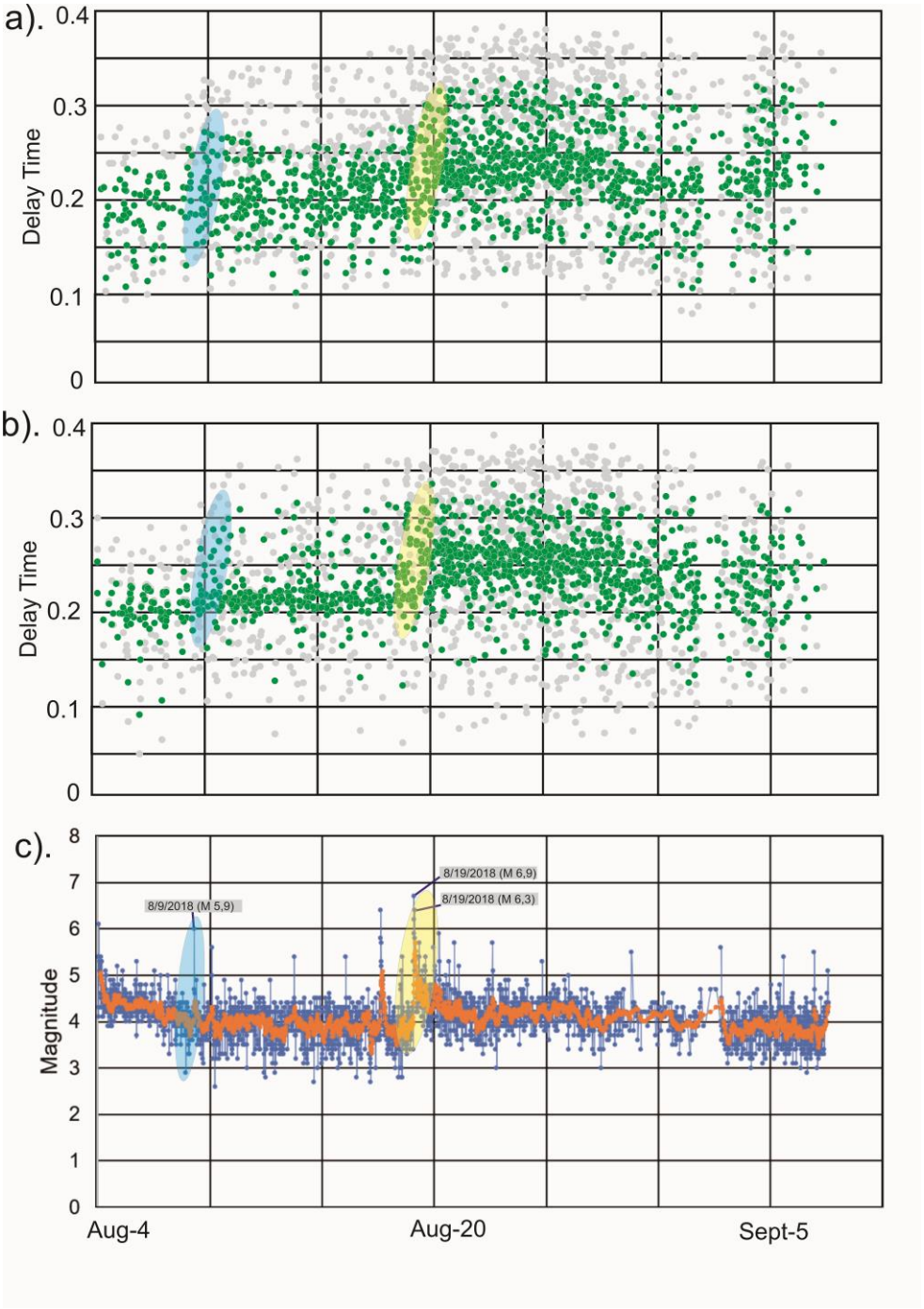

Fig. 6. a) Temporal variation in delay time at station LM05 ; b) Temporal variation in delay time at station LM06; c) Variation of earthquake magnitude respect to recording time. Blue oval symbols depict the trend correlation respect to August 9 (M 5.9) earthquake, and Yellow oval symbols show the correlation towards August 19 earthquakes magnitude

Supplementary Files

This is a list of supplementary files associated with this preprint. Click to download.

- SupplementalMaterialSWSinLombokEQSasmietal.pdf